A Statistical Analysis of Climate Sensitivity and Climate Forcing Across the Globe

REDACTED[a] (Supervisor: REDACTED)[a]

[a]McGill University

December 5, 2022

A 480 year time-series of climate forcing was determined for 1079 locations across the surface of Earth. To do so, the reciprocal of a parameter known as climate sensitivity was estimated for each location, as well as the global land average, estimated as 2.16 ± 0.24 Wm^{-2}/K. Finally, a global time-series of climate forcing was constructed and compared to previous estimates by government bodies.

Climate | Forcing | Statistical

Climate projections are of the utmost importance to guide science and policy to an effective solution to climate change. Specifically, precisely projecting quantities, especially temperature and information related to temperature, can give insights into a plausible future of the planet. Precision in estimates is key, as climate models utilize highly non-linear equations that are sensitive to minute uncertainties.[1] Modern methods of predicting such values rely heavily on deterministic, computational models, but such models are seeing diminishing returns.[2] As such, new methods of making climate predictions are needed. In particular, the research conducted for this project may be used in stochastic models that rely more on empirical measurements and statistics than computational brute force, as outlined in Lovejoy (2021).[1]

Climate data often suffers from a considerable amount of randomness,[1] thus research consisted of numerical and statistical analysis of said historical data. This included empirical measurements of geological data at numerous borehole locations around the planet, as well as reanalysis data produced via the climate models of The European Centre for Medium-Range Weather Forecasts (ECMWF). The importance of utilizing borehole data is that it is rarely used in similar climate predictions and thus allows for a novel comparison to current models. The research of this paper managed to produce historical values of climate forcing (discussed below) over several hundred years at numerous locations. The aggregate of these results was compared to current global estimates that have used far less direct methods, and may allow for more accurate climate predictions out to the year 2100.[2] Specifically, a comparison with IPCC (Intergovernmental Panel on Climate Change, a United Nations body) forcing estimates was made.[3]

1 Theory

The focus of this research was on finding historical values of the Earth's climate forcing. Climate forcing is the net radiative flux anomaly present at some strata of the Earth's atmosphere. If the stratum in discussion is the top of the atmosphere, the climate forcing is denoted F_{TOA}, and if the strata is the Earth's surface, the forcing is denoted F_{SUR}. A radiative flux anomaly is the deviation from the accepted baseline radiative flux. This baseline is the average, long term net radiative flux at a given location; that is, the average electromagnetic radiation flux through some portion of Earth's atmosphere. Any deviation from this baseline is called an anomaly, and it forces the energy balance at a given location out of equilibrium, hence the name "climate forcing." This forcing, over long enough timescales and large enough spatial regions, is a known affector of climate change.[3]

The fundamental equation governing this research was the following conservation equation:

$$F_{EXT} + F_{INT} = H + T/S \tag{1}$$

Here, the external (solar radiation, anthropogenic factors, etc.) and internal (radiation emitted by earth, but reflected back to the surface by clouds) climate forcing at a location are equated to the response of the climate system. Namely, how the temperature changes due to forcing (accounted for by the T/S term, with s being a scaling factor discussed below), and how heat is transferred down, into the surface of the earth, as well as transferred horizontally to other locations via conduction and convection (accounted for by the H term). All terms above are anomalies, so they are the deviations from their long term baseline values. Thus, even though the baselines may be large at some locations, the above terms are often small

relative to the baselines. At the scale of years, the H term is approximately equivalent to a simple heat flux.

To achieve these goals, a parameter known as climate sensitivity (S) was estimated. Climate sensitivity (S) is a parameter that determines the surface temperature response (T_{SUR}) due to a given forcing (F_{TOA}). This parameter is locally defined for a given location on the planet. Additionally, S was assumed to be relatively constant in time. For the purpose of this research project, the reciprocal of S was more important than S itself, and its averaged value across all 1079 boreholes was sought. Ultimately, determining S and 1/S is the same problem, but 1/S was found directly for simplicity. Due to a large amount of noise in the F_{TOA} and T_{SUR} data, determining a value of S at each borehole location, as well as a globally averaged value of S, required Haar analysis methods (see Procedures section). This value is given by Eqn. 2:

$$\frac{1}{S} = \frac{<\Delta F_{TOA}^2>^{1/2}}{<\Delta T_{SUR}^2>^{1/2}} \quad (2)$$

Upon determining 1/S, heat flux (Q_{Bore}) and temperature (T_{Bore}) data from 1079 boreholes was used to determine a yearly estimate of the climate forcing (F_{Bore}) at the borehole locations via Eqn. 3 (see Procedures section for further detail). Borehole data was collected and analyzed as presented in Cuesta-Valero et al. (2021).[4] Eqn. 3 simply states that the anomalous radiation flux at a borehole location is equal to the heat flux entering the ground plus the temperature response at that location (scaled by the inverse climate sensitivity). This is a simplified version of Eqn. 1. The result was a series of yearly forcing values for each borehole location that spanned 480 years.

$$F_{Bore} = Q_{Bore} + T_{Bore}/S \quad (3)$$

It is worth noting how and why Eqn. 1 was simplified to Eqn. 3. Eqn. 1 includes a term for the anomalous horizontal divergence of the heat flux within H. This term would account for the transfer of heat from a given location on the surface of Earth into another, rather than coming directly from the sun. This is an effect of heat imbalance caused by anthropogenic factors occurring over the past few decades. However the anomalous horizontal divergence of the heat flux was assumed to be negligible over the majority of the 480 year series due to said anthropogenic factors only occurring recently. As for the more recent decades, this term was estimated to be significantly smaller than the components included in Eqn. 3.

2 Procedures

2.1 Inverse Climate Sensitivity

In order to determine the inverse climate sensitivity, we utilized ERA5 reanalysis data from the ECMWF (denoted by subscript RE for reanalysis). The ECMWF is a research institute that utilizes supercomputing and observational data to produce both meteorological forecasts and reanalyses.[5] This data is provided in an online catalogue. A reanalysis in this context is a constructed dataset of historical meteorological data that is not directly observed, but is instead derived from limited historical observations and computational methods. These are essentially weather forecasts but run backwards in time, painting an accepted image of past climate data dating back to 1959.[6] ERA5 is the latest iteration of this reanalysis data.

This dataset, analyzed in the Python and Mathematica programming languages, provided the surface temperature (T_{RE}) data and top-of-atmosphere forcing (F_{RE}) data needed to compute the inverse climate sensitivity (1/S) both locally and globally. However, due to noise in the dataset, the values for inverse climate sensitivity required careful treatment. While linear regression of F_{RE} and T_{RE} data could produce a value of S according to Eqn. 4 (a simplified version of Eqn. 2), the results were often unphysical.

$$F_{RE} = \frac{T_{RE}}{S} \quad (4)$$

This posed a fundamental issue to the research. In order to overcome this, the Haar fluctuations of F_{RE} and T_{RE} were analyzed and used according to Eqn. 2. The use and validity of Haar fluctuations to compute relevant parameters is presented in Lovejoy, 2012.[7] A Haar fluctuation of a quantity v(x), denoted Δv, is simply defined by Eqn. 5:

$$\Delta v = \left(\frac{1}{\Delta x/2}\int_{x}^{x+\Delta x/2} v dx\right) - \left(\frac{1}{\Delta x/2}\int_{x+\Delta x/2}^{x+\Delta x} v dx\right) \quad (5)$$

This is simply the mean of v(x) over the interval [x, x + Δx/2] minus the mean of v(x) over the interval [x + Δx/2, x + Δx]. Here, Δx is a given "lag" over which a Haar fluctuation is computed.

In terms of the forcing fluctuations, we have ΔF_{RE} discretely computed over a given lag of Δt. This lag was a timescale, which was restricted to an integer number of years (as fluctuations over yearly values were sought). Δt values ranging from 1 to 63 were valid since our data spanned the 63 years from 1959 through 2021. For reasons discussed below (see Fig. 6 and Discussion section), only

Δt values ranging from 16 through 33 years were used. For a given Δt, as many ΔF_{RE} were computed as there were Δt that fit in the 63 year interval. For Δt = 16, 3 ΔF_{RE} values were computed despite not spanning the entire interval. For Δt = 21, 3 ΔF_{RE} values were computed which did span the interval. After a set of ΔF_{RE} were computed by starting from 1959, an additional set of ΔF_{RE} were computed by starting from 2021 and moving backwards in time. See Fig. 1 and Fig. 2 for a pictorial representation of the process.

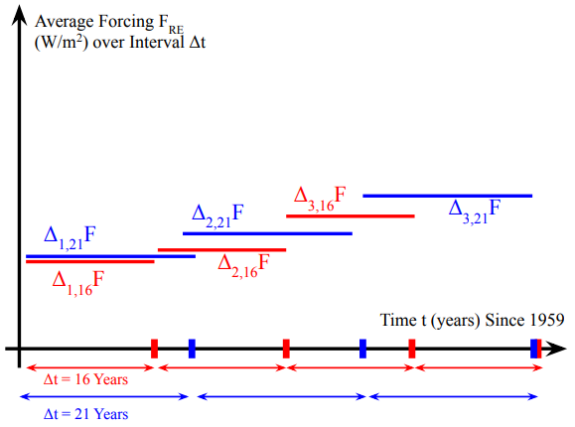

Figure 1: Haar fluctuations of two separate Δt values computed from the start of the time-series until the end. There are only as many fluctuations that fit within the 63 year interval. Each $\Delta_{i,j}F_{RE}$ is a continuous subset of F_{RE} spanning a given number of years j. The subsets of ΔF_{RE} were disjoint for a given Δt. The index i simply enumerates an individual Haar fluctuation corresponding to a given Δt.

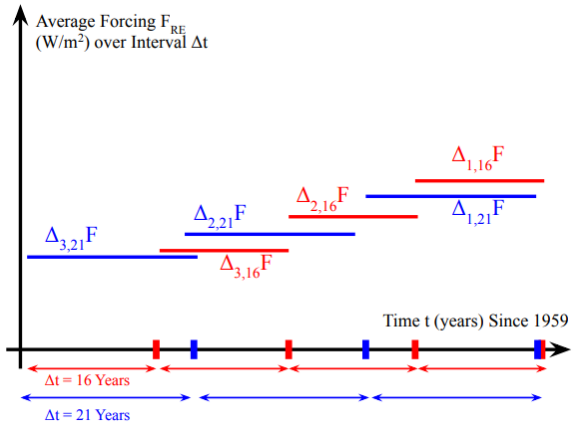

Figure 2: Haar fluctuation of the same Δt values as Fig. 1, but computed backwards from the end of the time-series until the start. Again, there are only as many fluctuations that fit within the 63 year interval.

Note that although the subset of ΔF_{RE} values corresponding to a given Δt are disjoint in a given forwards or backwards computation, there are still overlapping intervals of Δt when comparing both forwards and backwards computation. For example, the blue intervals present in Fig. 1 and Fig. 2 are identical. Regardless, this is in line with treatment presented in Lovejoy, (2012).[7]

An identical treatment of T_{RE} was conducted, and the root-mean-square (RMS) of these Haar fluctuations were computed. Finally, the ratio of these results were computed, giving Eqn. 2. This process was repeated for each borehole to produce location specific 1/S values. Finally, in order to produce the global $1/\overline{S}$ value of 2.16 ± 0.24 Wm^{-2}/K the average yearly value of top-of-atmosphere forcing (according to the reanalysis) across all the boreholes was taken, and this new 63 year series was used in the Haar computations. The uncertainties quoted in both the local and global 1/S values were determined by the standard error-in-the-mean formula given in Eqn. 6:

$$\alpha_{1/S} = \frac{\sigma_{1/S}}{\sqrt{N-1}} \tag{6}$$

Here, N is the number of samples taken, i.e. the number Haar fluctuations used to compute 1/S.

2.2 Climate Forcing

The forcing series for each borehole location F_{Bore} was produced using the borehole-specific 1/S values in tandem with the Q_{Bore} and T_{Bore} series provided by Cuesta-Valero et al. (2021).[4] This data, analyzed in python, consisted of two CSV files for each borehole location (one for heat flux data, and another for temperature data). The combined dataset allowed for a continuous 480 year time series of forcing at each borehole. However, the different time series did not start and end at uniform dates, as different boreholes had data for different years. Additionally, the temporal resolution for each series was ~30 years on average, with identical Q_{Bore} and T_{Bore} values attributed to each year in a given ~30 year subset. This was simply the result of Cuesta-Valero et al. (2021).[4]

Upon averaging the forcing series (over all the boreholes) to produce an estimate of the global climate forcing, the temporal resolution increased to a nearly yearly resolution (a result of each individual borehole's 480 year series beginning and ending at different times). The result was a forcing series spanning from 1449 through 2015.

Finally, this global estimate was compared with the IPCC estimate for climate forcing which spans from 1750 to 2019, as well as two estimates (spanning from 1959 to 2021) constructed from ERA5 data. The first of these estimates was simply the ERA5 top-of-the atmosphere forcing (F_{RE}) data averaged over all borehole locations, with its baseline adjusted to that of global borehole estimate. The second estimate constructed from ERA5 data was produced via Eqn. 7:

$$\overline{F}_{ERA5} = \overline{T}_{RE}/\overline{S} \quad (7)$$

Here, the ERA5 averaged temperature data ($\overline{T}_{RE}$) was combined with the globally averaged inverse climate sensitivity determined by the Haar methods outlined above. This estimate ignored heat flux Q as it was not present in the ERA5 dataset, and there wasn't an overlap of Q_{Bore} data for the entire ERA5 time period. This was justified due to heat flux values presented in the borehole data being ~20 times smaller than temperature T/S contribution.

Finally, the IPCC forcing was altered in 2 different ways and compared again with our research findings. It is important to state that the IPCC estimated the forcing by combining individual estimates of forcings (for each year, 1750 to 2019) caused by separate factors. Of note, the IPCC had a forcing contribution attributed to volcanic events, and another attributed to aerosol pollution in the atmosphere. So, the first alteration was to reduce the forcing contribution due to volcanic events via Eqn. 8. This transformation does not alter the mean value of the volcanic contribution over the series, but changes yearly contributions as outlined by Procyk et al. (2022).[8] And second, the IPCC forcing contribution due to aerosols was removed, as ERA5 data and thus our borehole forcing did not take them into account (see Discussion section).

$$F_{Vol,0.3} = < F_{Vol} > (F_{Vol})^{0.3} / < F_{Vol}^{0.3} > \quad (8)$$

3 Results

An estimate of 1/S and a forcing profile (here, profile simply means curve) were made for each of the 1079 boreholes (see Fig. 3 for one such profile). In addition, a global estimate of $1/\overline{S}$ was found to be 2.16 ± 0.24 Wm^{-2}/K. From this estimate, a global forcing profile was generated from the borehole data and compared against other estimates (see Fig. 4 and Fig. 5) as discussed above.

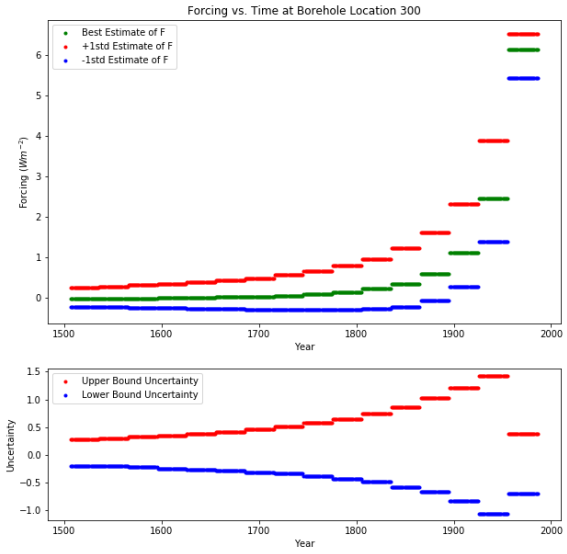

Figure 3: An example of the climate Forcing as a function of date at latitude and longitude (47.61, -69.46). This is located along the QuebecMaine border. Forcing is displayed at 30-year resolution (the same resolution present in the borehole data).

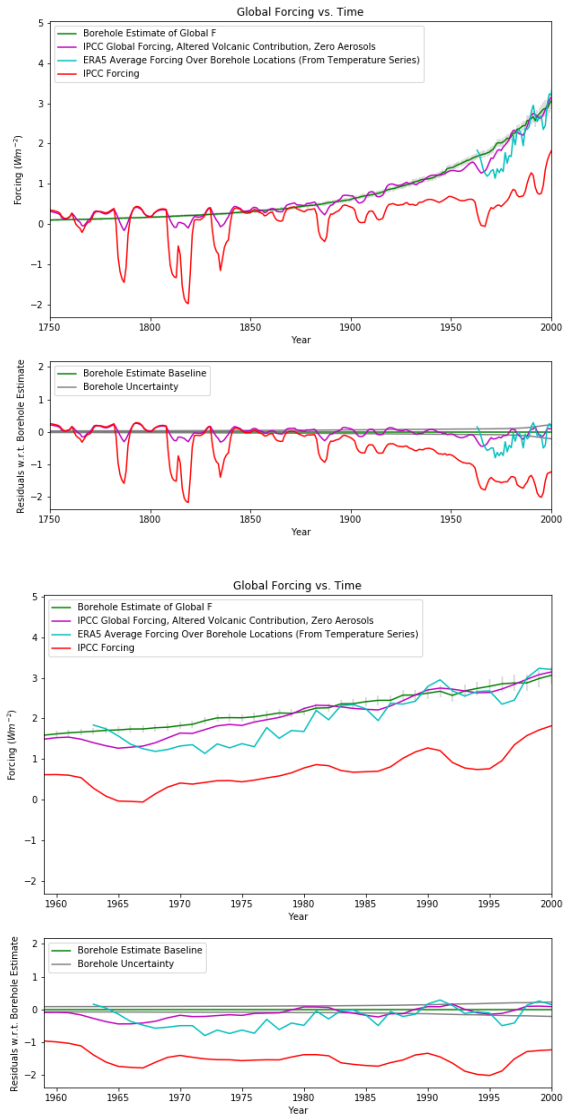

Figure 4: Four forcing profiles are present in each plot with residuals w.r.t. the borehole forcing profile. The right plot (1959 - 2000) is a zoomed in version of the left plot (1750 - 2000). A 5-year running average has been computed over the IPCC and ERA5 profiles. Borehole uncertainty is shaded grey. Purple profile: the IPCC forcing profile with zero aerosol contributions and with volcanic contributions altered according to Eqn. 8. Blue profile: ERA5 forcing profile generated according to Eqn. 6. Red profile: the IPCC forcing profile as presented by the IPCC themselves.[3] The baseline of the IPCC profiles were defined by setting the mean forcing values of the borehole series and the IPCC series equal to one another over the years 1750 through 1850, as nearly no anthropogenic factors contributed to forcing during this period and thus all forcing results should theoretically be consistent. The baseline of the ERA5 profiles were defined by setting their means to that of the boreholes over the period 1959 through 2015 (the full period of overlap).

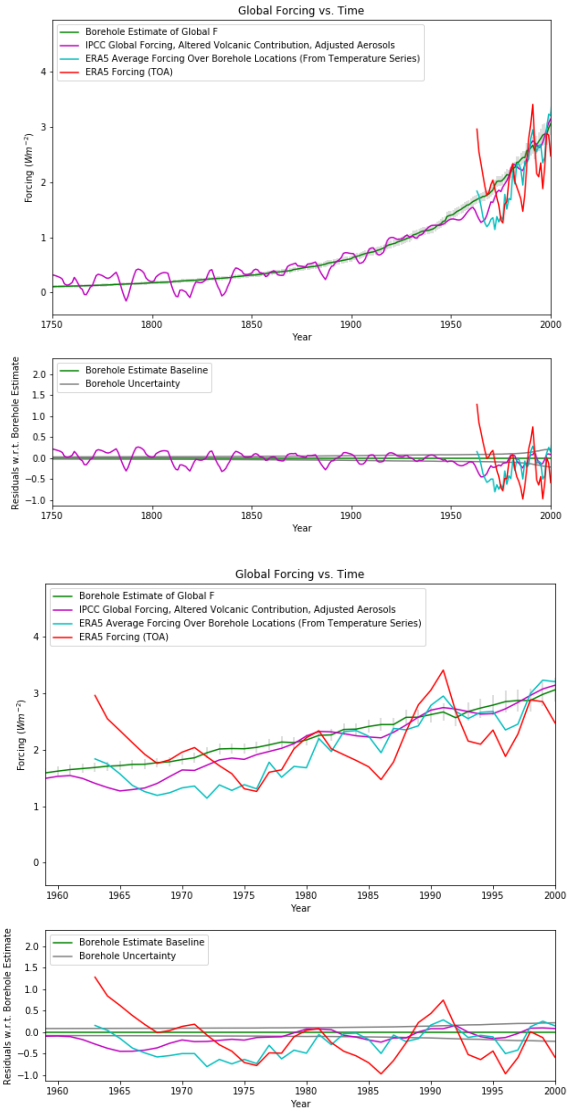

Figure 5: The same plots as Fig. 5 are repeated here, but the red profile has changed to be the ERA5 top-of-atmosphere forcing (taken directly from the ERA5 catalogue).

It is evident from the figures above that climate forcing began to increase significantly during the industrial revolution, starting roughly around 1800, and growing much faster starting in the 1900s. It is also evident that the borehole forcing estimate is, on average, greater than the unaltered IPCC forcing estimate (see Fig. 4, red profile), but upon removing the aerosol contribution the two estimates have better agreement (see Fig. 4 and Fig. 5, purple profile).

In addition to determining climate forcing profiles, an interesting discovery was made regarding the 1/S estimates. Namely, that the value of 1/S (determined through Haar fluctuation analysis) varied depending on the timescales (Δt) used in the Haar fluctuations; in other words, depending on the timescales over which the forcing and temperature response were observed (see Fig. 6).

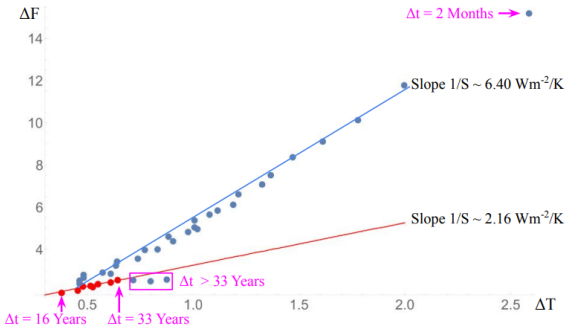

Figure 6: $1/\overline{S}$ values are computed as the slopes of 2 lines-of-best-fit (via linear regression). Restricting $\Delta\overline{F}$ components to those of widths between 16 and 33 provides a 1/S result (see red line) that represents long-term climate (inverse) sensitivity. Such forcing is the cause of long-term climate change rather than intermediate weather patterns. Widths greater than 33 years were neglected due to there only being 1 disjoint subset of F for those timescales (and thus less reliable statistics). No error is quoted for individual data points as ERA5 did not report error in their estimates. Instead, error is quoted in the slope (± 0.24 Wm^{-2}/K) due to uncertainty in the regression.

4 Discussion

Our results are best discussed under the scope of correlations. Below are the correlations between the global borehole forcing profile and the other profiles present in Fig. 4 and Fig. 5.

IPCC Profile (Unaltered)	IPCC Profile (Altered Volcanic, No Aerosols)	ERA5 Profile (Derived from Eqn. 7)	ERA5 Profile ($\overline{F}_{TOA}$ Data)
~ 0.60	~ 0.97	~ 0.70	~ 0.44

Table 1: For each profile present in Fig. 4 and Fig. 5, the correlation coefficient w.r.t. the global borehole profile is given.

It is evident that our borehole profile (see Fig. 4) is most strongly correlated to the IPCC profile that doesn't include aerosols (see Fig. 7) and has reduced volcanic contributions. This reflects the fact that the purple profile in Fig. 4 and Fig. 5 more closely resembles the borehole profile than any other. The ERA5 correlations reflect the vast amount of noise present in the ERA5 forcing estimates. This was entirely the reason that Haar fluctuation analysis was applied to the ERA5 data in the first place. In addition, the top-of-atmosphere ERA5 data strongly reflects the forcing variability over short timescales. As such, this noise is not really noise, but reflects the alternate 1/S value in Fig. 6, which is a consequence of internal factors such as clouds, rather than external, climate changing factors. This explains the increased correlation of the ERA5 profile that only accounts for the forcing corresponding to the 1/S parameter for long timescales. Finally, the unaltered IPCC profile exhibits significantly less correlation than the altered IPCC profile.

To investigate the IPCC profile's correlation further, we analyzed the correlation coefficients of multiple (alternate) IPCC profiles w.r.t. the globally averaged borehole temperature profile. This analysis focuses solely on the temperature correlation because, within our global forcing profile given by Eqn. 3, the $T_{Bore}\sqrt{\overline{S}}$ term dominates the Q_{Bore} term by more than an order of magnitude.

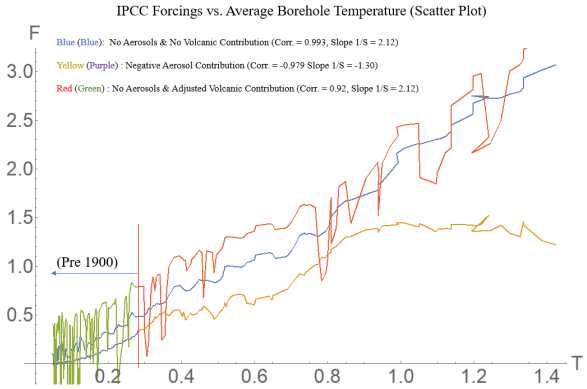

Figure 7: The top curve is the IPCC forcing with reduced volcanic contribution and without any aerosol contribution. The middle curve is the IPCC forcing without any volcanic or aerosol contributions. The bottom curve is purely the aerosol contribution to the forcing, with no other forcing contributions. This final curve is inverted (negative) for the sake of displaying in the same quadrant as the other two profiles. A distinction is made between data preceding and succeeding 1900. The later period exhibits a rapid increase in forcing and temperature.

Fig. 7 provides the following correlations between three IPCC forcing profiles as well as the $1/\overline{S}$ values estimated via regression with the global borehole temperature profile:

IPCC Profile (Altered Volcanic, No Aerosols)	IPCC Profile (No Volcanic, No Aerosols)	IPCC Profile (Pure Aerosol)
~ 0.92	~ 0.99	~ -0.98
2.12 Wm^{-2}/K	2.12 Wm^{-2}/K	-1.30 Wm^{-2}/K

Table 2: For each IPCC forcing variation present in Fig. 7, the correlation coefficient w.r.t. the global borehole profile is given (row 2), as well as the 1/S value estimated from the data in Fig. 7 (row 3).

Evidently, the global borehole temperature estimate is extremely positively correlated with the IPCC profile that excludes volcanic and aerosol forcing contributions, while it is extremely negatively correlated with the IPCC profile for the aerosol contribution. In addition, the negative correlation corresponds to a negative $1/\overline{S}$ value. This implies that an aerosol contribution cannot be readily distinguished from a lesser 1/S value. This poses a question, as to how one might definitively account for aerosol contribution to climate forcing, as well as determine an accurate 1/S value without muddling the two. This was beyond the scope of this research, but addressing this issue with Bayesian statistics, as discussed in Procyk R. et al. (2022)[9] would likely be a fruitful approach.

5 Conclusion

The general trend present across the majority of boreholes was that climate forcing increased significantly over the past centuries, and the majority of this increase has transpired since 1900. This is to be expected given the overwhelming evidence that the current state of climate change is a consequence of human developments.[3]

What is interesting is how the borehole forcing profile in Fig. 4 shows, on average, a greater forcing than the unaltered IPCC estimate. This is primarily a result of the IPCC's estimate of the effect of aerosols on the effective global climate forcing. Indeed, the effect of aerosols is to cool the Earth, and thus lessen the net forcing seen at any point on Earth.[3] The borehole forcing profile does not take aerosols into account, as the $1/\overline{S}$ estimate relied on ERA5 data that also did not account for aerosols, thus the only fair comparison could be made with an IPCC profile that did not include aerosol contributions.

Regarding the value of 1/S, it was found that the temperature over a given region was less sensitive to internal forcing anomalies due to rapidly changing factors such as clouds. In contrast, temperature was more sensitive to forcing anomalies that occurred over longer timescales (where the Δt components of Haar fluctuations were greater than 15 years). This was a key discovery, as it is the long-term (inverse) sensitivity that is responsible for climate change (and specifically, climate change due to anthropogenic forcing).[3] It was this longer-timescale value that was quoted as 2.16 ± 0.24 Wm^{-2}/K.

6 Acknowledgments

My sincerest thanks to Professor **REDACTED** for his consistent guidance and vast amount of time he devoted to this project. It was his expertise in this area of study that made this project possible. I'd also like to thank Professor Hugo Beltrami, St. Francis Xavier University for allowing us to use his team's research and borehole data. And finally, a thanks to my friend **REDACTED** (a McGill master's student) who sat through many long meetings conducted for the sake of this project.

7 References

1. Del Rio Amador, L., and Lovejoy, S., 2021: Using regional scaling for temperature forecasts with the Stochastic Seasonal to Interannual Prediction System (StocSIPS), Clim. Dyn., 1432-0894, doi: 10.1007/s00382-021-05737-5
2. Lovejoy S., 2022: The future of climate modelling: Weather details, macroweather stochastics—or both?, Meteorology;1(4):414–449.
3. IPCC, 2022: Climate Change 2022: Impacts, Adaptation, and Vulnerability. Contribution of Working Group II to the Sixth Assessment Report of the Intergovernmental Panel on Climate Change [H.-O. Pörtner, D.C. Roberts, M. Tignor, E.S. Poloczanska, K. Mintenbeck, A. Alegría, M. Craig, S. Langsdorf, S. Löschke, V. Möller, A. Okem, B. Rama (eds.)]. Cambridge University Press. Cambridge University Press, Cambridge, UK and New York, NY, USA, 3056 pp., doi:10.1017/9781009325844.
4. Cuesta-Valero et al., 2021: Long-term global ground heat flux and continental heat storage from geothermal data, Clim. Past, doi: 10.5194/cp-17-451-2021
5. About home. ECMWF. 2017 Aug 24 [accessed 2022 Dec 3]. https://www.ecmwf.int/en/about
6. Climate reanalysis. ECMWF. 2013 Dec 17 [accessed 2022 Dec 3]. https://www.ecmwf.int/en/research/climate-reanalysis
7. Lovejoy, S., and Schertzer, D., 2012: Haar wavelets, fluctuations and structure functions: convenient choices for geophysics, Nonlin. Processes Geophys., doi: 10.5194/npg-19-513-2012
8. Procyk, R. et al., 2022: The fractional energy balance equation for climate projections through 2100, Earth Syst. Dynam., 13, 81–107, 2022, doi: 10.5194/esd-13-81-2022, p.86.
9. Procyk, R. et al., 2022: The fractional energy balance equation for climate projections through 2100, Earth Syst. Dynam., 13, 81–107, 2022, doi: 10.5194/esd-13-81-2022, p.87.